Byun, J., Toksöz, M. N., Analysis of the acoustic wavefields excited by the Logging-While-Drilling (LWD) tool .
International Symposium on the Fusion Technology of Geosystem Engineering, Rock Engineering and Geophysical Exploration
Seoul, Korea, Nov. 18-19, 2003

Analysis of the acoustic wavefields excited by the Logging-While-Drilling (LWD) tool

Joongmoo Byun, M. Nafi Toksöz
Massachusetts Institute of Technology, Cambridge, U.S.A.

Abstract: Synthetic seismograms recorded with a logging-while-drilling (LWD) tool in the presence of slow formation are computed by the discrete wavenumber method. Monopole, dipole, and quadrupole logging tools are simulated with a source center frequency of 4 kHz. The modes in the responses are identified and characterized with time and frequency semblance plots. Numerical results show that, to obtain the formation shear velocity, we need to correct the peak velocities of the multipole modes in the semblance plots by using analytical dispersion curves.

1. Introduction

Logging-while-drilling (LWD) tools, designed to attach to the drill collar, are receiving attention due to their advantages in engineering and economics. By carrying out logging while drilling, we can improve sonic measurements while avoiding formation alteration (e.g. mud cake) or hole enlargement problems that arise occasionally in wireline logging performed after drilling. In addition, real time measurements of rock acoustic properties will provide a precursor for a possible overhead pressure zone ahead of the drill bit. The schematic diagram of the LWD tool is shown in Fig. 1.

Unlike a wireline logging tool, a LWD tool occupies the major part of a fluid-filled borehole and its sources and receivers are located close to the borehole wall. This geometry has a significant effect on excited acoustic wavefields in the borehole and yields different waveforms at the receivers from its wireline counterpart. In addition, the narrow fluid region between a tool and a formation requires very fine size grids in the numerical simulation with the finite difference method.

In this study, we examine the acoustic wavefields excited in a fluid-filled borehole with a LWD tool for slow formation (soil). We simulate waveforms received at monopole, dipole, and quadrupole LWD loggings using the discrete wavenumber method (Cheng and Toksöz, 1981; Tubman et al., 1984; Schmitt and Bouchon, 1985), which avoids the grid size problem. By using time and frequency domain semblance analyses, we identify the modes included in waveforms, and extract the formation shear velocities.

2. Logging-While-Drilling (LWD) tool

Wireline tool vs. LWD tool

In a monopole wireline tool, an omni directional pressure source transmits a compressional wave pulse in a borehole fluid. This compressional energy converts compressional and shear waves in the formation around the borehole when they hit the borehole wall. If both compressional and shear velocities of the formation are greater than the fluid velocity of compact rock (called *fast* or *hard formation* in logging), the compressional and shear energy in the formation returns the tool as refracted waves. The formation compressional and shear velocities can be measured with these refracted waves. However, in some poorly consolidated rock or soil, the formation shear velocity is less than the borehole fluid velocity (called *slow* or *soft formation* in logging). In this situation, the refracted shear waves do not occur in the borehole fluid, thus we cannot measure the formation shear velocity with refracted shear waves. Muiltipole (e.g., dipole, quadrupole) sources were proposed and developed to overcome this problem in measuring the shear velocity in slow formation. Interface modes excited by the multipole source, e.g., the flexural mode from a dipole source and the screw mode from a quadrupole source, are dispersed and have the same speed as the formation shear velocity at low frequency in both fast and slow formations. A wireline tool is modelled as a solid layer within the borehole in numerical simulation. Its presence has the same effect as those obtained from reducing the borehole size and increases the cut-off frequencies of the modes (Cheng and Toksöz, 1981). Therefore, the tool is not sometimes considered in the numerical simulation.

A LWD tool is significantly different from a wireline tool in two respects. First, a LWD tool divides the borehole fluid into two fluid columns and introduces additional modes (e.g. tool flexural mode, inner fluid Stoneley mode) that can be excited by logging sources. The dispersion characteristics of the modes are governed mainly by the properties of the associated layer. However, there are regions where dispersion curves of modes associated with different layers intersect. The resulting dispersion plot has the modes exchanging their dispersion characteristics above or below the intersection point (Rao et al., 1999). Fig. 2 shows a dispersion curve when a LWD tool is in the borehole. All material properties and borehole size are the same as in Fig. 1. We can see the interaction between the tool flexural mode and the borehole flexural mode around 1000 Hz. Secondly, a LWD tool occupies the major part of the cross section area of the borehole and the tool cannot be ignored in the numerical simulation. A LWD geometry is modelled as four layers: inner fluid, tool, outer fluid, and formation.

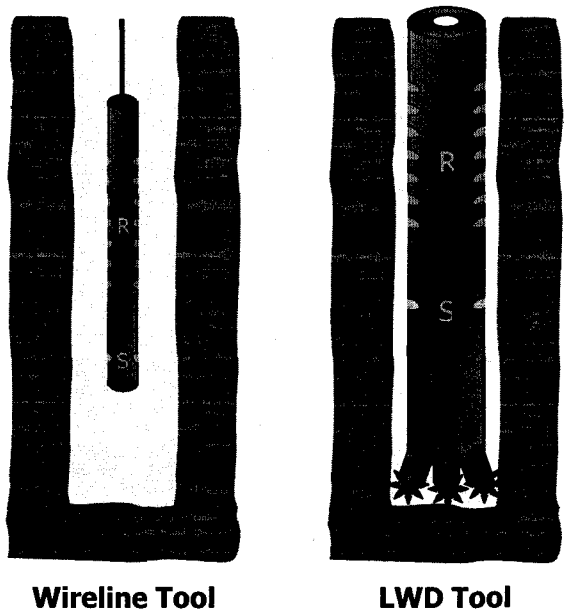

Fig. 1. The schematic diagrams of the LWD and wireline tool.

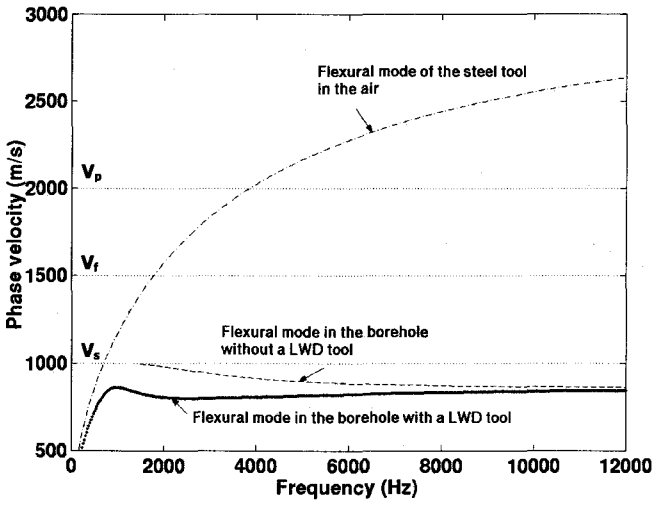

Fig. 2. Dispersion curves of the flexural modes in the borehole surrounded by slow formation with and without a LWD tool. V_p, V_s, and V_f are the formation compressional, shear velocities, and fluid velocity, respectively.

Constructing multipole sources and acquiring multipole components

Kurkjian and Chang (1986) showed that a multipole source of order n could be constructed from $2n$ monopoles (point sources) placed in the same horizontal plane. The monopoles are positioned periodically along the circle and alternate in sign. In addition, they pointed out that an array of pressure sensors on the axis of the borehole would only sense the monopole component of an acoustic field. They concluded that a sensor which responds to the n^{th} radial derivative of the displacement potential would sense only the n^{th} order multipole component of the acoustic field in the borehole. That is, we need to deploy an array of horizontal displacement sensors on the axis of the borehole to receive the dipole component of an acoustic field, and we need the spatial derivative of displacement for quadrupole component.

In a LWD system, the dipole source is constructed of two point sources of opposite sign (Fig. 3 (b)) and a quadrupole source is constructed of four point sources of alternate sign at right angles to each other (Fig. 3 (c)). A monopole source can be implemented by four point sources of the same sign (Fig. 3 (a)). The monopole and multipole components can be acquired by subtracting or adding the responses at four monopole receiver arrays. If we call responses at receiver arrays A, B, C, and D, depending on their locations associated with point sources (shown in Fig. 3), the dipole component can be obtained by A-C, the quadrupole component by A-B+C-D, and the monopole component by A+B+C+D, respectively.

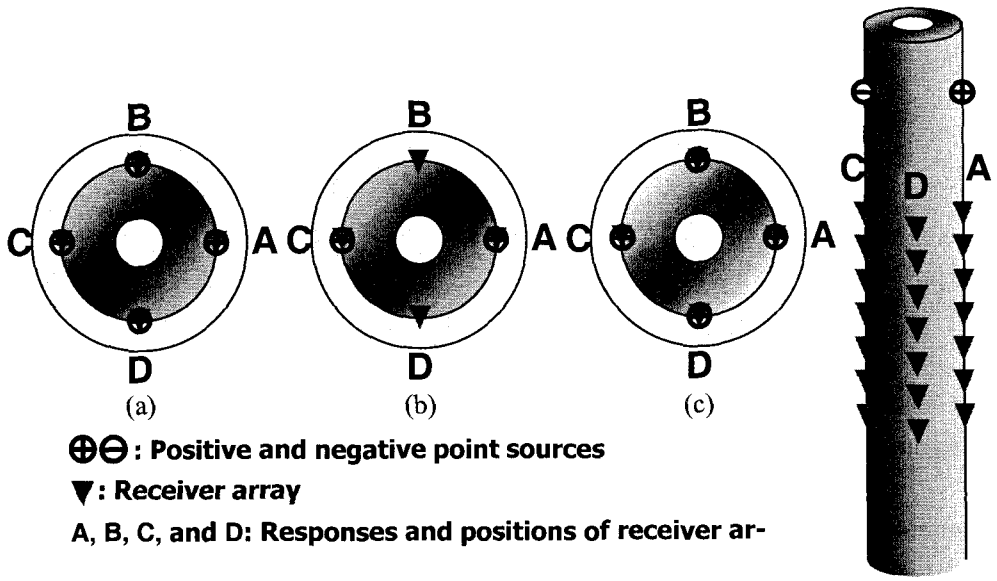

Fig. 3. Construction of a monopole, dipole, and quadrupole source with point sources.
(a) Monopole source (b) Dipole source (c) Quadrupole source

3. Three-dimensional wave propagation in a fluid-filled borehole

In this study, the response at each receiver array due to a multipole source was calculated based on the response due to an off-centered point source. For example, in the case of a dipole source, the response of one receiver array was obtained by combining the response due to the positive point source of the dipole source and the response due to the negative point source of the dipole source. To evaluate the 3D field generated by an off-centered point pressure source in a fluid-filled borehole, we followed Tadeu's work (1992). Consider a cylindrical fluid-filled borehole buried in a homogeneous elastic medium of infinite extent. For a harmonic point pressure source at position $(x_0,0,0)$, oscillating with a frequency ω, the incidence field can be expressed by using dilatational potential ϕ:

$$\phi_{inc}(t,x,y,x)=\frac{A\exp\left[i\frac{\omega}{\alpha}\left(\alpha t-\sqrt{(x-x_0)^2+y^2+z^2}\right)\right]}{\sqrt{(x-x_0)^2+y^2+z^2}} \quad (1)$$

where A is the wave amplitude, α is the compressional wave velocity of the fluid containing the source, and $i=\sqrt{-1}$.

Defining the effective wavenumbers

$$k_\alpha = \sqrt{\frac{\omega^2}{\alpha^2} - k_z^2}, \qquad \mathrm{Im}\, k_\alpha < 0 \tag{2}$$

$$k_\beta = \sqrt{\frac{\omega^2}{\beta^2} - k_z^2}, \qquad \mathrm{Im}\, k_\beta < 0$$

with the axial wavenumber, k_z, and Fourier transforming equation (1) in the z direction, one obtains

$$\phi_{inc}(\omega, x, y, k_z) = \frac{-iA}{2} H_0^{(2)}\left(k_\alpha \sqrt{(x-x_0)^2 + y^2}\right) \tag{3}$$

where the $H_n^{(2)}(\cdots)$ are the Hankel functions of the second kind and order n. However, equation (3) expresses the incident field in terms of waves centered at the source point (x_0,0,0), and not at the axis of the borehole. By Graf's addition theorem (Watson, 1980), the incident potential in equation (3) can be rewritten in terms of waves at the origin in the cylindrical coordinates:

$$\phi_{inc}(\omega, r, \theta, k_z) = \frac{-iA}{2} \sum_{n=0}^{\infty} (-1)^n \varepsilon_n H_n^{(2)}(k_\alpha r_0) J_n(k_\alpha r) \cos(n\theta) \tag{4}$$

when $r < r_0$

$$\phi_{inc}(\omega, r, \theta, k_z) = \frac{-iA}{2} \sum_{n=0}^{\infty} (-1)^n \varepsilon_n H_n^{(2)}(k_\alpha r) J_n(k_\alpha r_0) \cos(n\theta) \tag{5}$$

when $r > r_0$

where the $J_n(\cdots)$ are Bessel functions of order n, θ is the azimuth, and

$$\varepsilon_n = \begin{cases} 1 & \text{if } n = 0 \\ 2 & \text{if } n \neq 0 \end{cases}$$

$r = \sqrt{x^2 + y^2}$ is the radial distance to the receiver,

r_0 is the radial distance from the cylindrical axis to the source, and

$\cos\theta = x/r$, $\sin\theta = y/r$.

In the (ω, k_z) domain, the scattered fields in the solid formation can be written in a similar form to that of the incident field:

$$\begin{aligned} \phi_{sca}^s(\omega, r, \theta, k_z) &= \sum_{n=0}^{\infty} A_n H_n^{(2)}(k_{\alpha_s} r) \cos(n\theta) \\ \psi_{sca}^s(\omega, r, \theta, k_z) &= \sum_{n=0}^{\infty} B_n H_n^{(2)}(k_{\beta_s} r) \sin(n\theta) \\ \chi_{sca}^s(\omega, r, \theta, k_z) &= \sum_{n=0}^{\infty} C_n H_n^{(2)}(k_{\beta_s} r) \cos(n\theta) \end{aligned} \tag{6}$$

where ψ and χ are shear potentials that satisfy a wave equation with a shear wave velocity β. A_n, B_n, and C_n are unknown coefficients to be determined from appropriate boundary conditions. Index s indicates that the wave velocities of the *solid* formation must be used. The scattered field in the fluid can be expressed as

$$\phi_{sca}^f(\omega, r, \theta, k_z) = \sum_{n=0}^{\infty} D_n J_n(k_{\alpha_f} r) \cos(n\theta) \tag{7}$$

where index f indicates the fluid, and

$$k_{\alpha_f} = \sqrt{\frac{\omega^2}{\alpha_f^2} - k_z^2}.$$

D_n is also determined from boundary conditions. The total field inside the borehole fluid is the sum of the incident field and the scattered field in the fluid:

$$\phi_{tot} = \phi_{inc} + \phi_{sca}^f \tag{8}$$

4. Numerical results

Acoustic fields excited by monopole, dipole, and quadrupole sources in a LWD tool geometry were examined for slow formation. Table 1 shows the material properties and geometry used in the numerical simulation. For a source wavelet, we used a Ricker wavelet with a center frequency of 4 kHz. To avoid tool body waves, all point sources and receivers were located inside the annulus between the steel tool and the formation, 5 mm away from the steel tool. In a real LWD tool, sources and receivers are implemented on the tool, and attenuators (e.g. rubber) are inserted between sources and receivers to prevent tool body waves. Therefore, the results from sources and receivers in the annulus can be corresponded to the ideal implementation of the attenuators.

Table 1. Model parameters for a dipole LWD simulation.

	Formation (slow)	Tool (steel)	Borehole fluid
V_p (m/s)	2000	5940	1500
V_s (m/s)	1000	3220	0
Density (g/cm^3)	2.0	7.84	1.0
Tool inner radius (m)		0.024	
Tool outer radius (m)		0.092	
Borehole radius (m)		0.108	
Source-1st receiver offset (m)		1.37	
Receiver spacing (m)		0.15	
Number of receivers per array		7	

Monopole source

As mentioned in the previous section, monopole components are obtained by summing the responses at all receiver arrays in a real LWD logging survey. We followed the same procedure in the simulation. First, we obtained responses at each receiver array due to a dipole source. To acquire synthetic waveforms at receivers, we computed the responses in the frequency range from 0 to 20 kHz. Then, we summed responses at all arrays to acquire monopole component. The resulting seismograms and their frequency spectrums are shown in Fig. 4 (a) and (b), respectively. The spectrum shows the maximum at around 2.5 kHz. Modes included in the responses and their phase velocities are analysed by semblance calculation in time domain. From the time semblance plot in Fig. 4 (c), we observe three arrivals. The first arrival travels at the formation compressional velocity, 2000 m/s. This arrival is a refracted compressional wave. The second arrival travels at the formation shear velocity. This is a leaky shear wave. In the wireline case, the leaky shear is very weak in a slow formation and is often covered by noise or other arrivals. The leaky shear arrival in LWD case is still weak, but observed more because source and receivers are close to the formation (Huang, 2003). The third arrival is a Stoneley wave traveling at a velocity (about 800 m/s) slower than the formation shear velocity. The modes can be more clearly identified in the semblance plot in the frequency domain. Fig. 4 (d) shows the frequency semblance plot obtained by Nolte et al.'s method (1997). Black circles indicate the phase velocity of the maximum semblance in each frequency. The pink line shows the analytical dispersion curve of the Stoneley wave. The peak of frequency semblance follows the Stoneley mode up to 7 kHz and it shows the leaky shear mode at higher frequencies. When we compare the frequency semblance plot to the time semblance plot, we can find that the peak velocity of the Stoneley mode (about 800 m/s) in the time semblance plot agrees with the phase velocity of the Stoneley mode at the frequency (about 2.5 kHz) which has the maximum amplitude in the spectrum.

Dipole source

Fig. 5 shows the dipole component obtained by A-C with a dipole LWD tool. In a time semblance plot, we observe compressional arrival and the flexural mode. However, the leaky shear is not clear in this case. The frequency semblance shows that the response includes a $n = 3$ mode as well as the flexural mode. As shown from the semblance plots, we cannot obtain the formation shear velocity from the flexural mode directly. Unlike dipole wireline logging, we need to apply the correction on the peak of the flexural mode by using analytical dispersion curves to acquire the formation shear velocity. Although the leak shear gives the formation shear velocity, it is very weak and it does not guarantee that we can always observe the leaky shear from the data.

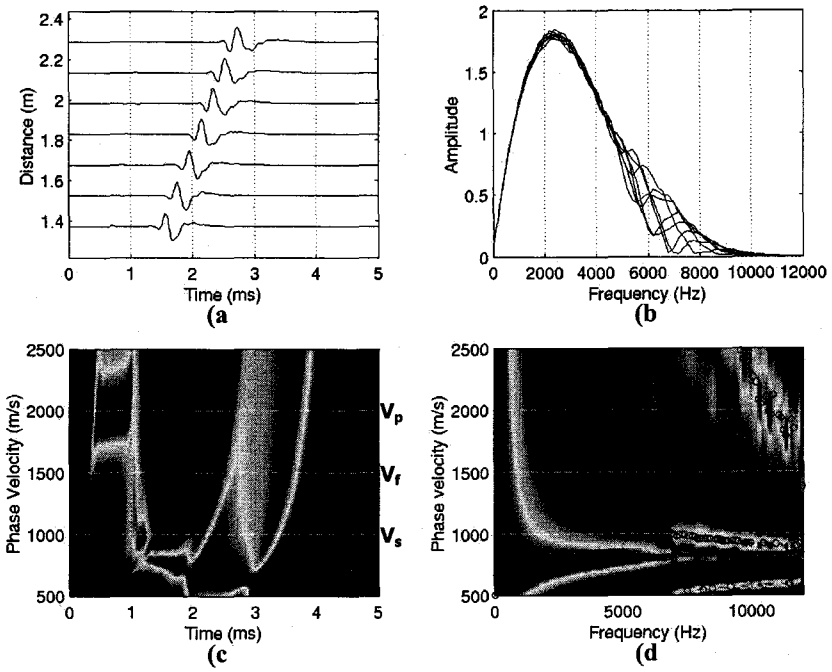

Fig. 4. Monopole response (A+B+C+D) of a monopole LWD tool in fluid filled borehole surrounded by slow formation. Black circles indicate the phase velocity of the maximum semblance at each frequency. The pink line shows the analytical dispersion curve of the Stoneley ($n = 0$) mode.
(a) Seismograms (b) Frequency spectrum (c) Time domain semblance plot (d) Frequency domain semblance plot

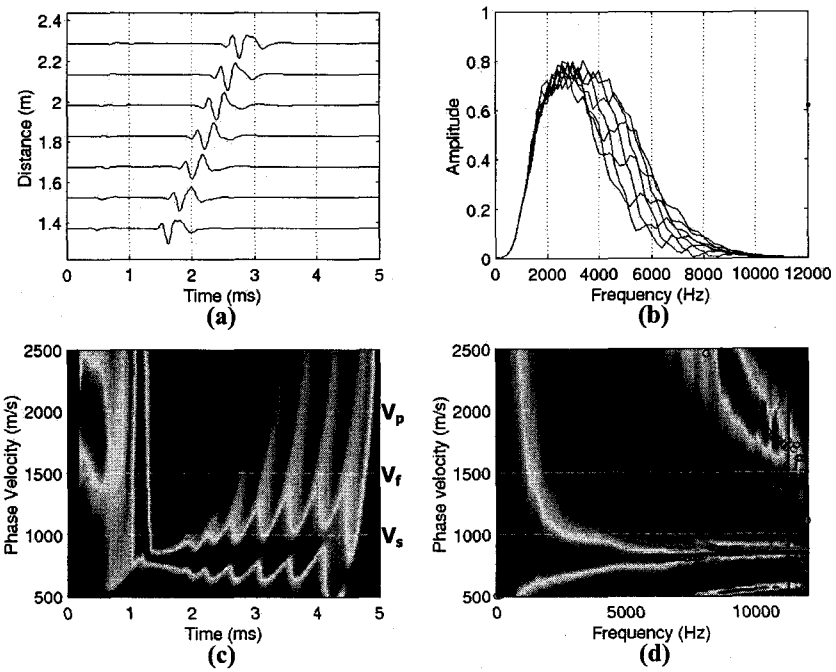

Fig. 5. Dipole response (A-C) of a dipole LWD tool in fluid filled borehole surrounded by slow formation. The pink line and the green line show the analytical dispersion curves of the flexural ($n = 1$) mode and $n = 3$ mode, respectively.
(a) Seismograms (b) Frequency spectrum (c) Time domain semblance plot (d) Frequency domain semblance plot

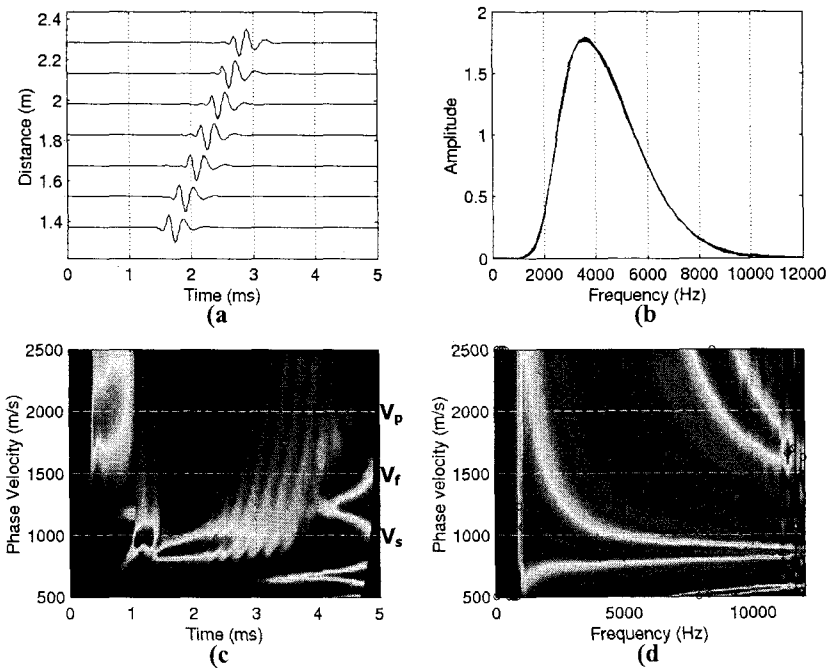

Fig. 6. Quadrupole response (A-B+C-D) of a quadrupole LWD tool in fluid filled borehole surrounded by slow formation. The pink line shows the analytical dispersion curves of the screw (n = 2) mode and n = 3 mode, respectively. (a) Seismograms (b) Frequency spectrum (c) Time domain semblance plot (d) Frequency domain semblance plot

Quadrupole source

Fig. 6 shows the quadrupole component obtained by A-B+C-D with a quadrupole LWD tool. We identify three arrivals: the compressional, the leaky shear, and the screw mode in the time semblance plot. The theoretical dispersion curve of the screw mode in the frequency semblance plot indicates that the borehole screw mode is not interfered by the tool screw mode in this frequency range. However, the peak of the screw mode in the time semblance plot is still less than the formation shear velocity and needs correction to acquire the formation shear velocity from it.

5. Conclusions

Logging-while-drilling can avoid problems associated with mud cake or a change in borehole size. Specifically, the real time processing of the LWD data will provide valuable information for drilling decisions made in the field.

Acoustic fields excited due to a monopole, dipole, and quadrupole sources in LWD geometry were simulated by the discrete wavenumber method. Monopole, dipole, and quadrupole sources were constructed from the combination of the point sources, and monopole, dipole, and quadrupole responses were acquired by subtraction or summation of the responses at four monopole receiver arrays.

Numerical results show that, unlike multipole wireline logging, the peaks of the flexural mode or the screw mode in the time semblance plots do not provide the formation shear velocity directly. Therefore, to acquire the formation shear velocity, we have to apply the correction on these peaks by using analytical dispersion curves.

References

Cheng, C. H., Toksöz, M. N., 1981, Elastic wave propagation in a fluid-filled borehole and synthetic acoustic logs, Geophysics, Vol. 46, 1042-1053.

Huang, X., 2003, Effects of tool positions on borehole acoustic measurements: a stretched grid finite difference approach, Ph.D. Thesis, Massachusetts Institute of Technology.

Kurkjian, A., Chang, S. K., 1986, Acoustic multipole sources in fluid-filled boreholes, Geophysics, Vol. 51, 148-163.

Nolte, B., Rao, R., Huang, X., 1997, Dispersion analysis of spilit flexural waves, M.I.T. Borehole Acoustics and Logging and Reservoir Delineation Consortia Annual Report.

Rao, R., Burns, D. R., Toksöz, M. N., 1999, Models in LWD applications, M.I.T. Borehole Acoustics and Logging and Reservoir Delineation Consortia Annual Report.

Schmitt, D., Bouchon, M., 1985, Full-wave acoustic logging: Synthetic microseismogram and frequency-wavenumber analysis, Geophysics, Vol. 50, 1756-1778.

Tadeu, A. J. B., 1992, Modeling and seismic imaging of buried structures, Ph.D. Thesis, Massachusetts Institute of Technology.

Tubman, K. M., Cheng, C. H., Toksöz, M. N., 1984, Synthetic full-waveform acoustic logs in cased boreholes, Geophysics, Vol. 49, 1051-1059.

Watson, G. N., 1980, A treatise on the theory of Bessel function, Cambridge University Press, Second Edition.